



Simulated Gravity Field Estimation for the Main Belt Comet 133P/Elst-Pizarro Based on a Satellite-to-satellite Tracking Mode

Shang-Biao Sun¹, Jian-Guo Yan^{1,2} , Wu-Tong Gao¹, Bo Wang¹, Zhen Wang², Mao Ye¹, and Jean-Pierre Barriot^{3,1}

¹ State Key Laboratory of Information Engineering in Surveying, Mapping and Remote Sensing, Wuhan University, Wuhan 430079, China; jgyan@whu.edu.cn

² Xinjiang Astronomical Observatory, Chinese Academy of Sciences, Urumqi 830011, China

³ Geodesy Observatory of Tahiti, University of French Polynesia, BP 6570, F-98702 Faaa, Tahiti, French Polynesia, France

Received 2022 July 19; revised 2023 June 1; accepted 2023 June 6; published 2023 July 31

Abstract

Most asteroids and comets are formed in the early stages of the solar system and therefore contain a wealth of information about their birth. The asteroid exploration mission planned in the coming years by China will likely target the celestial body named 133P/Elst-Pizarro (estimated diameter of about 4 km). The orbit of this asteroid stays within the asteroid belt, but nevertheless, it displays a comet-like dust tail. In this study, we used differential tracking data between two simulated probes and the data from an Earth station to estimate 133P gravity field model. This observation mode is similar to how the gravity field was estimated for large celestial objects in the GRAIL and GRACE missions, but here the object is the very small 133P asteroid. We compared the estimated gravity fields obtained for 133P from the satellite-to-satellite combined with the Earth-based two-way range-rate observation mode, with only the Earth-based two-way range rate mode. The results show that the accuracy of the low-degree (4 degree and order) estimate of the gravity field is improved by one order of magnitude by using the satellite-to-satellite combined with the Earth-based two-way range-rate observation mode with respect to the Earth-only tracking. Furthermore, another order of magnitude improvement in the gravity field solution is gained by decreasing the orbit altitude from 12 to 8 km.

Key words: gravitation – methods: data analysis – celestial mechanics – comets: general

1. Introduction

The United States, the ESA, and Japan have been very active in comet/asteroid exploration missions. Recent missions include the NEAR mission to asteroid Eros (Cheng et al. 1997), the Hayabusa mission to asteroid Itokawa (Yoshikawa et al. 2015), the Rosetta mission to comet 67P (Glassmeier et al. 2007), the Dawn mission to the asteroid Vesta and the dwarf planet Ceres (Russell & Raymond 2011), the Hayabusa2 mission to the asteroid Ryugu (Watanabe et al. 2017) and the OSIRIS/REX mission to asteroid Bennu (Lauretta et al. 2015). By estimating gravity field models of these small bodies, their material distribution and structure composition can be constrained for further research. Miller et al. (2002) estimated the 10th-degree gravity coefficients of Eros and determined its spin rate and period as well as the R.A. and decl. of its pole. Scheeres et al. (2006) obtained the 4th-degree gravity coefficients of Itokawa from a shape model and estimated its mass with an error of about 5% using optical and LIDAR data. Pätzold et al. (2016) estimated the gravitational mass (GM) and degree 2 coefficients of 67P using the tracking data from 2014, and concluded to a homogeneous interior and a reasonable porosity value for the comet nucleus. Godard et al. (2017) further estimated the 5th-degree gravity coefficients for 67P by estimating the multi-arc observation data from 2016 August to

September. Konopliv et al. (2014, 2018) estimated the 20th-degree gravity coefficient estimate for Vesta and the 18th-degree gravity field coefficient estimate for Ceres. Yamamoto et al. (2020) estimated the 10th-degree gravity field model of the Ryugu assuming on a global constant density of 1.19 g cm^{-3} through a spherical harmonic expansion of the shape model (Watanabe et al. 2019). Chesley et al. (2020) derived a 10° and order gravity field for Bennu by modeling the motion of dust particles ejected from the body by outgassing.

133P/Elst-Pizarro (hereafter 133P), like Bennu (Lauretta et al. 2019), has the properties of both an asteroid and a comet. 133P was discovered in 1979 (Elst et al. 1996) in the main asteroid belt between Mars and Jupiter. It was first given an asteroid number (7968 Elst-Pizarro), but it was found to have a tail of dust in 1996, a feature typical of comets (Boehnhardt et al. 1998). The dust tail of 133P was also observed in 2002 and 2013 (Hsieh et al. 2004; Jewitt et al. 2014). The current knowledge of the orbital parameters and physical properties of 133P are summarized in Tables 1 and 2.

Tables 1 and 2 list the parameters involved in the simulation experiments. Back-and-forth communication delays between spacecraft and Earth can reach hours, which are incompatible with emergency maneuvers (Leonard et al. 2012). These observation data from Earth are also impacted by the Earth

Table 1
Orbital Parameters of 133P (JD 2457400.5)

Parameter	Value
Observation arc	13,350 days (36.55 yr)
Aphelion	3.66751 au (548.652 Gm) (Q)
Perihelion	2.6524 au (396.79 Gm) (q)
Semimajor axis	3.1600 au (472.73 Gm) (a)
Eccentricity	0.16062 (e)
Orbital period (sidereal)	5.62 yr (2051.7 days)
Average orbital speed	16.64 km s ⁻¹
Mean anomaly	187°70 (M)
Mean motion	0° 10 m 31.656 s day ⁻¹ (n)
Inclination	1°3873 (i)
Longitude of ascending node	160°14 (Ω)
Argument of perihelion	131°97 (ω)
Jupiter MOID	1.51427 au (226.532 Gm)
T_{Jupiter}	3.185

atmosphere and ionosphere, as well as by interplanetary plasma, especially during conjunctions, reducing the precision of navigation and orbit determination.

Onboard tracking modes such as onboard optical tracking, radio tracking ranging and radar/laser ranging are immune to these problems. Onboard optical tracking is the method by which the probe observes the landmarks on the surface of the celestial body. Onboard radio tracking is ranging or Doppler between the orbiter and a lander (Ye et al. 2021), while radar/laser ranging is performed between the spacecraft and the body surface (Chang et al. 2016). The observation data from these observation modes are widely used and analyzed to enable autonomous navigation and orbit determination in deep space exploration, especially in case of non-visibility with Earth stations (Turan et al. 2022a). The inter-satellite observation mode has not yet been implemented in small-bodies exploration missions.

In this work, we focus on the satellite-to-satellite tracking mode, associated with an Earth “standard” radio-tracking. More precisely, a ground station communicates with “probe A” orbiting the asteroid and tracking measurements are taken between “probe A” and “probe B.”

Many researchers have focused on this observation mode. Yim et al. (2004) verified the feasibility of this approach by simulating inter-satellite range measurements. Psiaki (2011), Leonard et al. (2012), Liu et al. (2014), Benedetti et al. (2019), and Genova & Petricca (2021) explored the application of this tracking mode in theoretical cases (large and small planetary bodies). Zuber et al. (2013) constructed the 420th degree and order moon gravity field model using the early satellite-to-satellite tracking observations from the GRAIL mission. With the accumulation of this type of observation, the lunar gravity field model had been estimated to degree and order 1500 (Park et al. 2015). However, the method must be simulated and

Table 2
Physical Properties of 133P

Parameter	Value
Dimensions	3.8 ± 0.6 km (Hsieh et al. 2009) 3.9 ^{+0.4} _{-0.3} km (Yu et al. 2020)
Mean density	1.3 g cm ⁻³ (Hsieh et al. 2004)
Synodic rotation period	3.471 hr (0.1446 day) (JPL)
Geometric albedo	0.074 ± 0.013R
Temperature	160 K (Hsieh et al. 2004)
Apparent magnitude	17.24 to 20.71
Absolute magnitude (H)	15.6 (JPL) 15.3R (Hsieh et al. 2004) 15.49R (Hsieh et al. 2010)

analyzed in depth, and a series of validation experiments must be performed before carrying out an actual exploration mission.

A Chinese probe will be launched to the asteroid main belt in 2025 (announcement of China National Space Administration in 2019 April). Two small bodies will be targeted: the near-Earth asteroid 2016HO3, believed to be an excavated fragment of the Moon (Sharkey et al. 2021), and a main belt comet, that is not yet chosen at the time of this writing. 133P/Elst-Pizarro is one of the candidates, and 311P/PanSTARRS also known as P/2013P5 (Jewitt et al. 2013), is the other. According to the current plan, the probe will attach to the surface of the asteroid 2016HO3 to collect samples, and return the samples in a reentry capsule to Earth. The probe will continue on in its flight to approach the main belt asteroid with intermediate gravitational boosts by Earth and Mars.

The question is therefore: can this type of inter-satellite radio-tracking technique be applied to navigate around really a small, kilometer-sized body with a weak gravity field? This is the subject of this article, with a case study of the 133P comet. In Section 2, we present in full detail the method and force model used for the simulation. In Section 3, we present the results of the simulation with respect to the different tracking modes, orbit altitudes and noise levels (including ephemeris errors and solar radiation pressure errors). In Section 4 we draw conclusions and make recommendations for future missions.

2. Model and Methodology

We used the precise orbit determination software Small Body Precise Orbit Determination Toolkit (SPOT) developed by Wuhan University (Gao et al. 2023), as shown in Figure 1. The DOP853 algorithm was adopted for integration calculations. Finally, a least squares method was used to iteratively solve a solution.

Since the gravity field of 133P is weak, the other force models acting on the probe need to be accurately modeled. The inertial motion equation for the probe is

$$m\ddot{\mathbf{r}} = \mathbf{f}_{133P} + \mathbf{f}_{\text{NB}} + \mathbf{f}_{\text{SRP}} + \mathbf{f}_{\text{REL}} \quad (1)$$

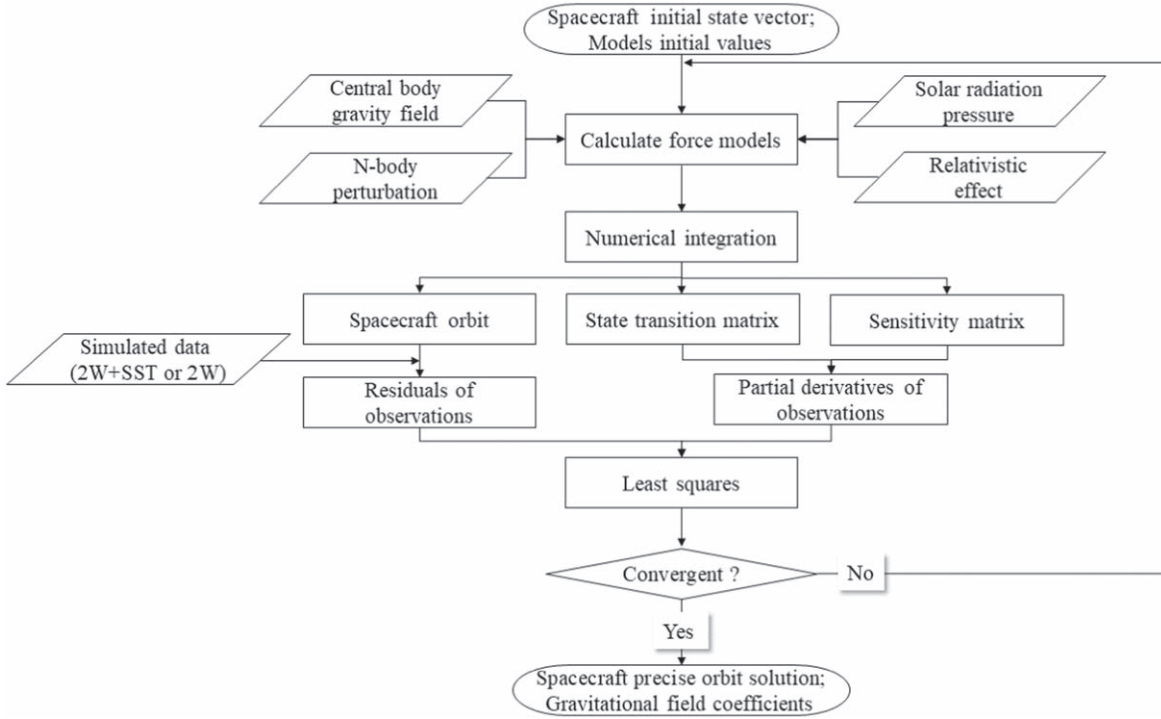


Figure 1. Flowchart of the internals of the orbitography software SPOT.

Table 3
Dynamical Model

Force Model	Descriptions	Order of Magnitude of the Acceleration (Altitude: 8 km; Unit:km s ⁻²)
Gravitational field of 133P	8th-degree gravity field model from the shape model and constant density	10 ⁻⁸
N-body perturbation	All point-mass perturbation bodies: Sun, eight planets, plus Pluto, Ceres, Vesta, and Pallas (DE431 ephemeris and JPL small body database browser)	10 ⁻¹⁴
Solar radiation pressure	Cannonball model (Montenbruck & Gill 2001), area-to-mass ratio 0.02 m ² kg ⁻¹ and solar radiation coefficient $C_r = 1.5$ for the two probes.	10 ⁻¹¹
Relativistic effect	Relativistic effect caused by Sun	10 ⁻¹⁵

where r is the position vector of the probe in the J2000 frame; m is the mass of probe; f_{133P} denotes the spherical and non-spherical perturbations of 133P, f_{NB} is the N -body perturbation, f_{SRP} is the solar radiation pressure, and the term f_{REL} is the relativistic effect of Sun on the probe.

For this simulation, the reference gravitational field (see Table A1 in the Appendix) was computed as follows: the even degree coefficients were calculated from a simple shape model assumed as an elongated triaxial ellipsoid with semi-axis $a > b = c$ ($a = 2.299$ km, $b = c = 1.654$ km) and a constant density ($\rho = 2.0$ g cm⁻³). The curve of the even degree spectrum was fitted using Kaula's rule (Kaula 1966). The gravity field coefficients were generated randomly based on the

fitted curve. Then we obtained the 8th-degree gravity field model of 133P using this approach which is shown in the Appendix. Descriptions of the dynamical model are shown in Table 3. The observation modes used in the simulation experiment are shown in Figure 2.

In Table 3, the configuration of each force model and corresponding parameter values are detailed. The gravity field of 133P plays the major role, followed by the solar radiation pressure; therefore, the gravity field coefficients and the solar radiation coefficient need to be considered.

There are two types of observation modes being used, as shown in Figure 2. The blue line indicates the two-way range rate observable (2W) between the ground station and probe A,

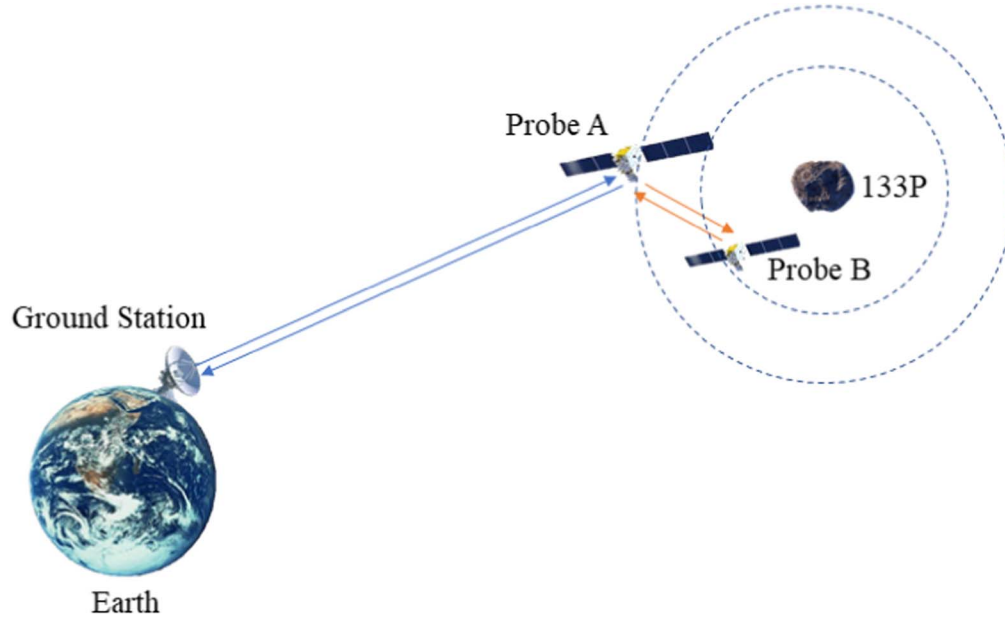


Figure 2. Schematic diagram of the two observation modes.

Table 4
Study Cases Considered in the Simulation

Case	Description	Parameter Setting
Case 1	Different Observation Modes	2W; 2W+SST
Case 2	Different orbital altitudes	8 km; 9 km; 10 km; 11 km; 12 km
Case 3	Different noise levels	10^{-3} m s^{-1} ; 10^{-4} m s^{-1} ; 10^{-5} m s^{-1}
Case 4	Different 133P ephemeris errors	0 km; 1 km; 5 km; 10 km
Case 5	Different solar radiation pressure coefficient C_r errors with 1.5	0; 0.05; 0.1; 0.2

and the orange line indicates the range rate observable (SST) between probe A and probe B.

The observation mode studied in this paper is a combination of Earth-based tracking and local tracking (around asteroids) and is denoted as 2W+SST. Earth-based tracking provides an absolute scale orientation of the system under study, because the orbit and orientation with respect to inertial space of Earth in the solar system are well documented, while local tracking will provide the differential (tidal) acceleration between the two probes. In order to assess the performance of this combination, five cases are listed in Table 4, which are analyzed separately according to the parameters in Table 5.

As can be seen from Table 4, the two observation modes are compared in case 1. The precision of estimating 133P's gravity model is used as a criterion. Based on the 2W+SST observation mode, a series of simulation experiments are designed to verify the effects of different orbital altitudes, noise levels, ephemeris errors and solar radiation pressure errors on estimating the gravity field model. The parameter variations that are investigated in these simulation experiments are listed

in the second to fifth cases of Table 4, respectively. For the comparison experiments, only the parameters in Table 4 were changed, and the other parameters in Table 5 were kept constant. In order to evaluate the effect on the small body gravity field solution after combining inter-satellite observations, the noise level is set to 0.1 mm s^{-1} for both inter-satellite and ground-based observations based on the analysis of the existing similar work (Eshagh & Šprlák 2016; Turan et al. 2022b). However, the noise level may be different in the actual exploration missions due to the design of the satellite system and the choice of payload. Therefore, in case 3, three different inter-satellite noise levels are set and the effects on the gravity field solution are analyzed. In addition, in order to reduce the accumulation of the force model error and close to real situation, we select an arc-length of one day.

For safety reasons (mainly dust collisions), orbits of sufficient altitude are needed. To ensure a full tracking coverage and illumination conditions on the comet surface, terminator circular orbits were chosen for both probes (McMahon et al. 2018). For consistency with the previous

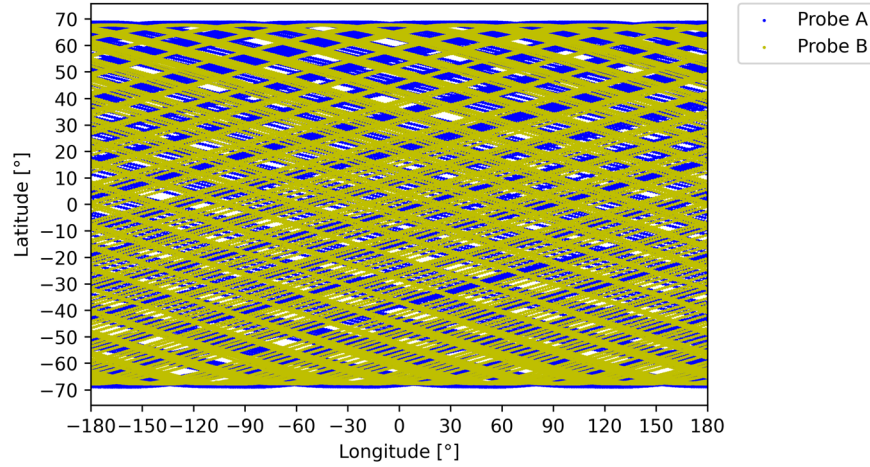


Figure 3. Coverage of two probes over a sphere co-rotating with respect to the comet 133P.

work of Gao et al. (2021b), who studied the modeling of the gravity field of 133P with a two- and four-way range rate observations mode between a single orbiter and lander, we selected the orbital altitude of probe A as the same as the initial altitude of the simulated orbiter (8 km) of the work of Gao. In addition, the priori uncertainties of the position and velocity of the initial orbit were also chosen to be 1 km and 1 m s^{-1} , respectively. We choose the initial altitude of the simulated probe B to be 0.5 km lower than for probe A, which increases the coverage of the sub-satellite point on the surface of 133P. We plotted the coverage of the two probes to verify the resonance effect.

As shown in Figure 3, since the orbits of the two probes have their periapsis on opposite sides of the 133P, their trajectories nearly full cover the sphere co-rotating with the comet. This indicates that no resonance effect is taking place in our simulation between the orbits of probe A and B and the gravity field of the comet.

3. Results

A series of simulation experiments were done to verify the accuracy of the 133P gravity field coefficient solutions. The accuracy of estimating the gravity field is assessed by the power spectra, which includes the rms coefficient sigma degree variance, σ_n and the rms coefficient error degree variances, δ_n and Δ_n . We choose the same criterion for our study. The formulas to calculated the values are as in

$$\sigma_n = \sqrt{\frac{\sum_{m=0}^n (\bar{C}_{nm}^2 + \bar{S}_{nm}^2)}{2n+1}}, \quad \delta_n = \sqrt{\frac{\sum_{m=0}^n (\sigma_{\bar{C}_{nm}}^2 + \sigma_{\bar{S}_{nm}}^2)}{2n+1}},$$

$$\Delta_n = \sqrt{\frac{\sum_{m=0}^n (\Delta_{\bar{C}_{nm}}^2 + \Delta_{\bar{S}_{nm}}^2)}{2n+1}} \quad (2)$$

where $\sigma_{\bar{C}_{nm}}$ and $\sigma_{\bar{S}_{nm}}$ are error variances of the gravity field coefficients \bar{C}_{nm} and \bar{S}_{nm} , respectively. The rms coefficient

Table 5
Parameters for the Simulation Experiments

Object	Description
Ground station	Kashi station in China
Observation mode	Two-way range rate, Two-way range rate + inter-satellite range rate
Range	0.1 m
Range rate noise level	Both modes of 10^{-4} m s^{-1}
Sampling interval	60 s
Cutoff angle/local horizon between the ground station and the probe A	10°
Initial orbital altitude	Probe A: 8 km, Probe B: 7.5 km
Initial inter-satellite range	2 km
Observation time	30 days
Number of arc segments	30

sigma degree variances show the “frequency” intensity of the gravity field model. The formal errors δ_n are retrieved from the posterior covariance matrix of the model. The true errors Δ_n are the difference between the solution and the “true” gravity field coefficients.

3.1. Comparison of Observation Modes

The 2W+SST observation mode was simulated according to the cases listed in Tables 4 and 5, with the inter-satellite range and range rate relative to a Doppler window of 60 s, computed over 30 days. We added Gaussian white noises with a mean value of 0 and standard deviations of 0.1 m and 0.1 mm s^{-1} for the inter satellite range and range rate, respectively.

As shown in Figure 4, given the different orbital altitudes, the range between both probes varies periodically between 0.2 and 16 km. The maximum inter-satellite range rate was about 0.2 m s^{-1} , with an average value of 0.1 m s^{-1} , which is one-hundred times larger than the set maximum noise level.

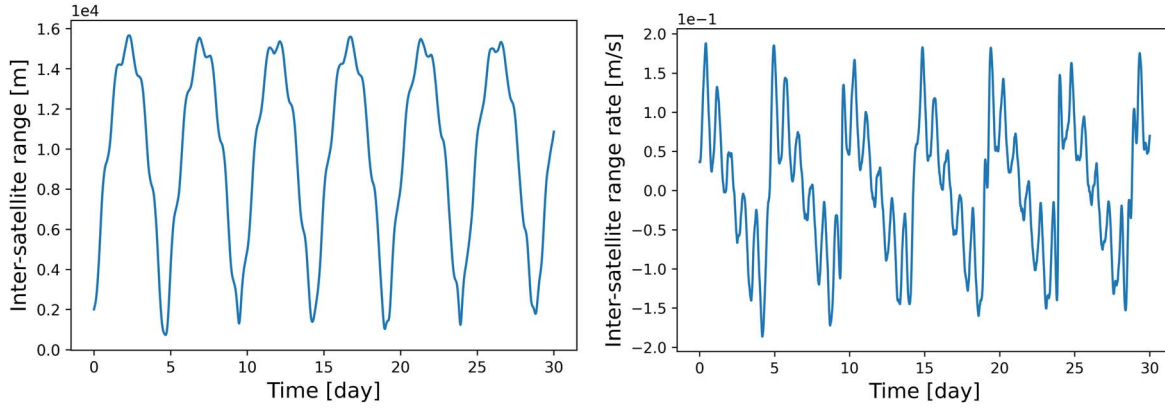


Figure 4. Range and range rate variations between probe A and probe B over 30 days according to Table 5.

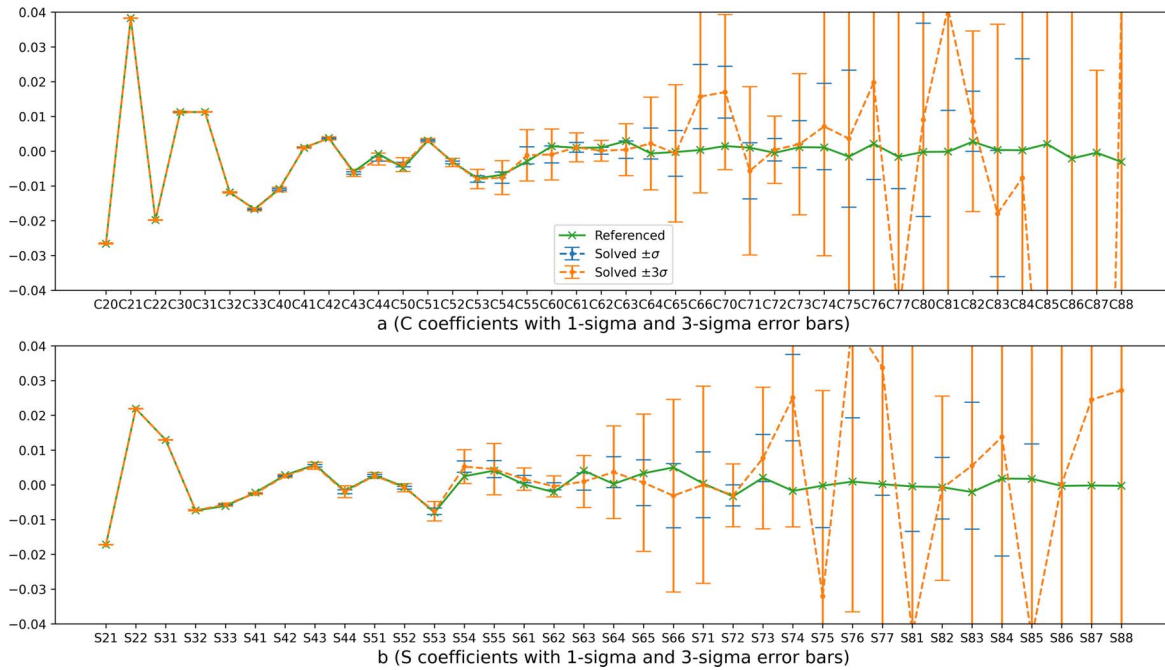


Figure 5. Modeled gravity coefficients (with error bars) with respect to “true” coefficients.

To visualize the results of estimating the 133P gravity field coefficients, we plotted the results with different error bars. Figure 5 shows the results of the solution model of the gravity coefficients of comet 133P, according to the settings of Table 5.

We can see that for the lower degrees, the estimated coefficients are very close to their reference “true” values and show small error bars, indicating these coefficients are well determined. However, as the degree increases, the uncertainty bounds gradually become larger, indicating that the result is not reliable.

In order to compare the differences in performances in gravity modeling between the different tracking modes, a single probe (with the same parameters as the probe A) was used to

perform two-way range rate measurements from a ground station. The two observation modes were compared by their degree rms magnitude spectra, as shown in Figure 6. The consistence between the formal error and the true error indicates the reliability of the solution. In the presence of systematic errors, such as ephemeris errors, it is difficult to tell how good the solution is using formal errors alone, which are related to the number of observations.

Figure 6 shows that the 2W observation mode permits only to estimate the gravity field up to degree 4. With the addition of SST data, degree 5 can be modeled, with an accuracy improved by an order of magnitude with respect to only 2W observations,

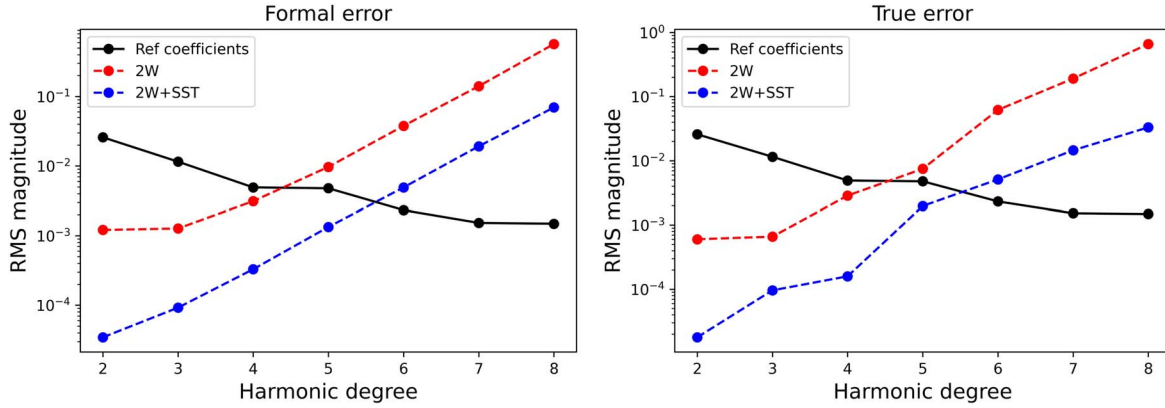


Figure 6. The degree rms magnitude spectra of the formal error and true error for case 1 listed in Table 4.

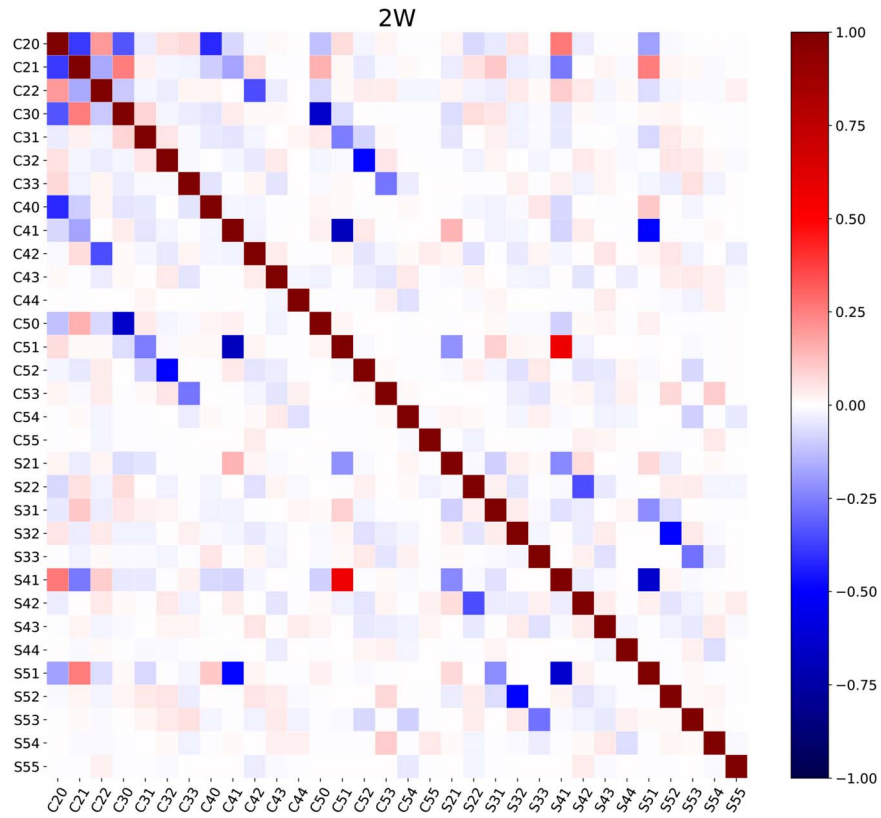


Figure 7. Correlations between the gravity field coefficients (\bar{C}_{nm} , \bar{S}_{nm}) of the 2W mode.

which is consistent with results in Figure 5. This is because the inter-satellite observation data are more sensitive to 133P's gravity field compared to the 2W observation data. For further analysis, the correlations between the gravity field coefficients of the three observation modes (2W; SST; 2W+SST) were calculated, as shown in Figures 7–9. As the maximum solution is up to the 5th degree gravity field model, we have only

computed correlation up to the 5th degree in order to show details.

As can be seen from Figures 7 and 8, there are large off-diagonal cross-correlations between the gravity field coefficients estimated by using only the 2W or SST observation data. When the 2W and SST observation data are combined, the correlations are greatly reduced, especially in the 2nd–4th

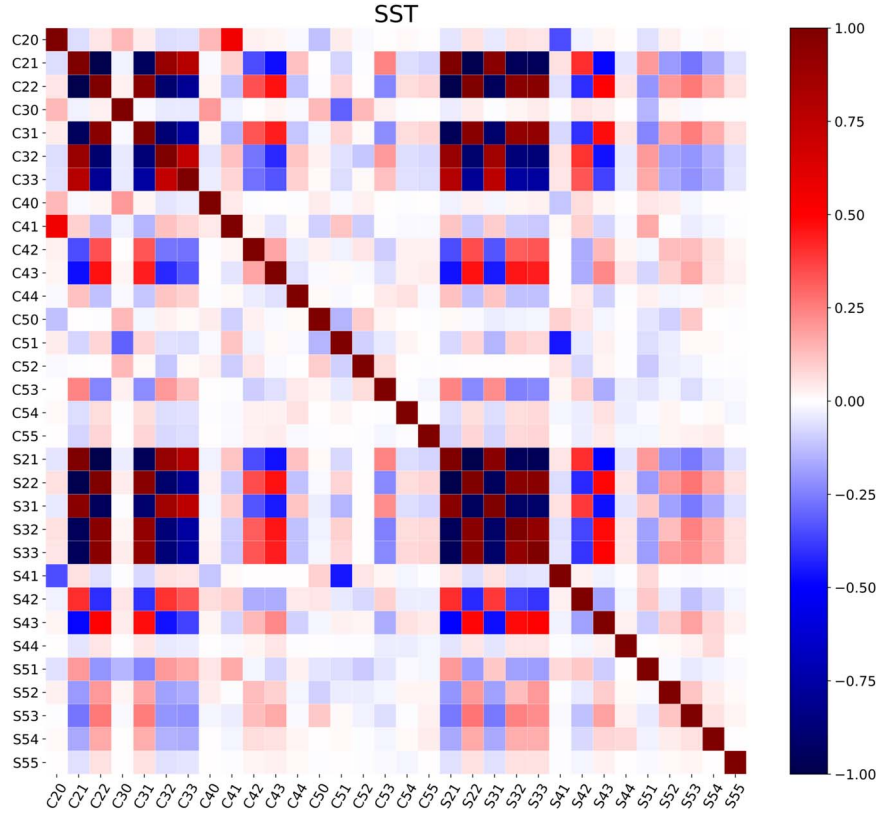


Figure 8. Correlations between the gravity field coefficients (\bar{C}_{nm} , \bar{S}_{nm}) of the SST mode.

degree and order terms, as shown in Figure 9. In addition, the inter-satellite data are more sensitive to the gravity field signal, a higher resolution gravity field model could be estimated. In the 2W observation mode, there are 13,300 observations, while the number of simulated observations in the 2W+SST observation mode is at least four times higher than that of 2W. In order to study the influence of the number of 2W observation data in the estimation of the gravity field, we extended the simulation time for a 2W observation mode-only up to 50 days. The results are shown in Figure 10.

As shown in Figure 10, although we have extended the observation time at the ground station to increase the amount of 2W observations, the improvement is not significant. This is because after 30 days, the sub-satellite points already cover the entire surface of 133P, as shown in Figure 3. Increasing the amount of data in 2W mode does not improve the estimation. Moreover, the inter-satellite range rate observations were generated even when probe A could not communicate with the ground station. To further understand this, the gravity field of 133P was estimated using only inter-satellite observations also, as shown in Figure 10. Although only the inter-satellite observation data were used, we could still estimate up to the fifth degree and order. However, the accuracy decreases at the 2nd–3rd degree and order term due to their large correlation, as

shown in Figure 8. As expected, due to the lack of ground station constraints, large deviations occurred when estimating the probe orbit, as shown in Table 6.

As can be seen from Table 6, the accuracy of the orbit estimated using only the range rate observation data between probe A and probe B was relatively low by an order of magnitude with respect to the 2W+SST observation mode. The observation data from the ground station does help to improve the precision of the orbits significantly toward the beginning of the observation processing and to reduce the uncertainty in probe state estimates. Leonard et al. (2012) gave the similar results on orbit determination using the satellite-to-satellite tracking mode. Therefore, during the actual exploration mission, the ground station must maintain communication with probe A to determine the absolute position of the probe and improve the accuracy of the orbit, while this does not affect too much the accuracy of the gravity field estimation.

3.2. Effects of Co-orbital Altitudes

Under the same observation conditions, the probes are affected by the asteroid gravity field differently at different orbital altitudes. The gravity pull of the asteroid increases when the orbital altitude is lower. Therefore, different altitude

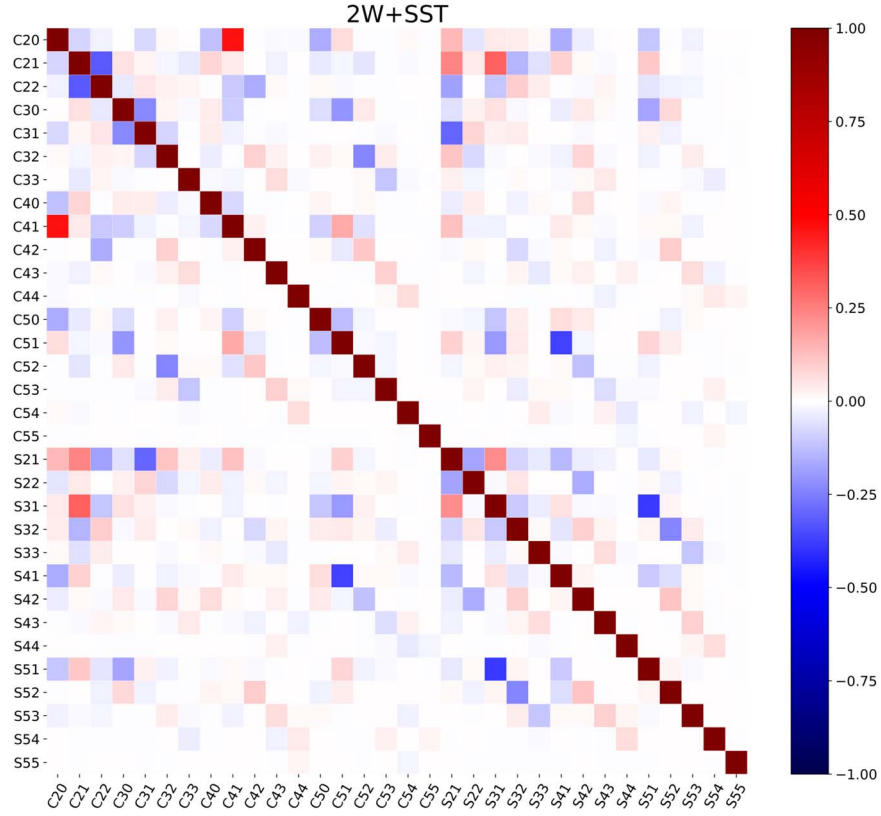


Figure 9. Correlations between the gravity field coefficients ($\bar{C}_{nm}, \bar{S}_{nm}$) of the 2W+SST mode.

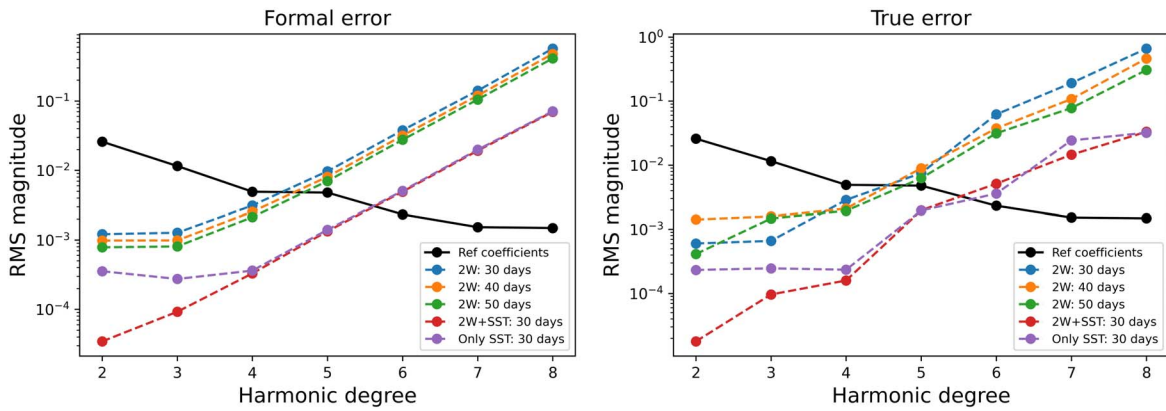


Figure 10. The degree rms magnitude spectra of the formal error and true error for different observation times.

choices are considered. The other settings in Table 5 are unchanged in this section; the results are shown in Figure 11.

As shown in Figure 11, as expected in the 2W+SST observation mode, the maximum degree of a possible gravity field estimation increases as the altitude decreases. When the orbital altitude is reduced from 12 to 8 km, the accuracy of estimating the gravity field model is improved by an order of magnitude. This orbit lowering is certainly constrained by security concerns. Observations with the Hubble Space

Telescope have demonstrated the presence of ice sublimation outgassing at the surface of 133P, which produces dust that can affect the probe (Jewitt et al. 2014). Therefore, the choice of orbit requires a trade-off analysis.

3.3. Effects of the Noise Levels

The observation noise often determines the quality of the inter-satellite observation data, which directly affects the

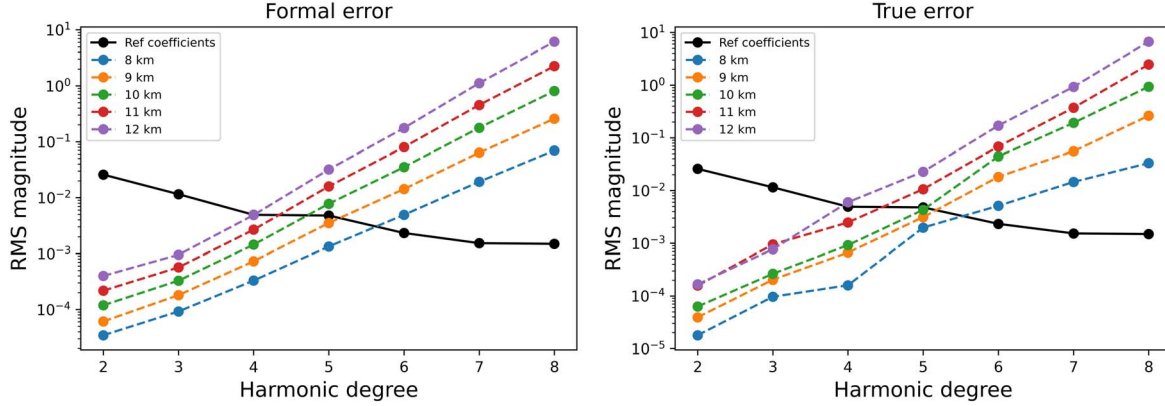


Figure 11. The degree rms magnitude spectra of the formal error and true error for case 2 listed in Table 4. The legend in the table shows the orbital altitude of probe A. The orbital altitude of probe B is 0.5 km lower.

accuracy of the gravity field solution. Here, we calculated the effect of three inter-satellite observation noise levels on the solutions, with results plotted in Figure 12.

As shown in Figure 12, when the observation noise of the SST observation mode was reduced from 10^{-3} to 10^{-5} m s^{-1} , the solution accuracy was improved by nearly two orders of magnitude. The level of miniaturization permissible for onboard electronics and pure physics limit the capacity to lower the noise levels and the three noise values used in the simulation are indicative.

3.4. Effects of 133P Ephemeris Errors

The ephemeris error on the 133P orbit was also considered. Gao et al. (2021b) assessed the influence of this error on the determination of rotation and gravity parameters in the two-way Earth-orbiter and orbiter-lander range rate tracking mode. To evaluate the impact of this error, the same approach was used. The ephemerides of 133P contaminated with 1, 5, and 10 km errors induced by an error in the timing of the ephemerides in the 2W+SST observation mode were used. The estimated gravity coefficients were compared with the corresponding results from gravity modeling with an unbiased 133P ephemeris, depicted in Figure 13.

As shown in Figure 13, the effect of ephemeris with different errors cannot be assessed based on the formal error alone, as the formal error is dominantly determined by the observation numbers. From the true error, the accuracy and maximum possible degree of the estimated gravity field in the 2W+SST observation mode decrease gradually with the increase of ephemeris error. However, a one-km error has no significant effect on the 2W+SST solution. A one-km accuracy for the ephemeris is certainly achievable when jointly estimating the gravity field and ephemeris. These results are consistent with the results estimated by combining the simulated orbiter-lander observation data of Gao (Gao et al. 2021b).

Table 6

Formal Error and True Error of the Position and Velocity Vector of the Probe

Object (km; km s^{-1})	Only SST		2W+SST	
	Formal Error	True Error	Formal Error	True Error
x0	0.023089	0.006683	0.006415	-0.00999
y0	0.059375	0.060732	0.001844	-0.00291
z0	0.014028	0.012725	0.002465	0.003824
vx0	1.61E-06	-1.87E-06	2.45E-07	2.69E-07
vy0	5.48E-06	5.54E-06	1.68E-07	-2.73E-07
vz0	9.95E-07	1.01E-06	4.85E-07	8.04E-07

3.5. Effects of Solar Radiation Pressure Errors

The effect of the solar radiation pressure force on the estimation of the gravity field needs also to be considered, especially for a probe equipped with large solar panels. The complexity in shape of solar panels, differences in reflective properties, as well as solar activity, make difficult to accurately model this perturbation force. In this work, we used a simple cannonball model with a solar radiation pressure coefficient C_r to be estimated, as

$$a_{\text{SRP}} = -PC_r \frac{A}{m} \frac{r}{r^3} \text{au}^2 \quad (3)$$

where P is the solar radiation pressure, C_r is the solar radiation pressure coefficient, A is the cross-sectional area of the solar panels, m is the mass of the probe, r is the distance from the Sun to the probe, and au is the astronomical unit. We evaluate the effect of Cr with different errors on estimating the gravity field model in the 2W+SST observation mode.

The “true” value of C_r was fixed at 1.5, and we added for the simulation four levels of error to the “true” value of C_r : 0.05,

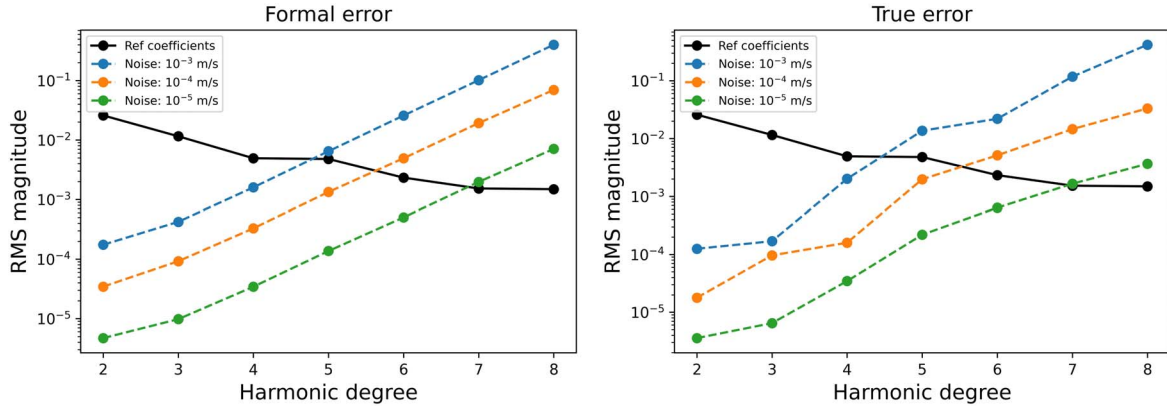


Figure 12. The degree rms magnitude spectra of the formal error and true error for case 3 listed in Table 4.

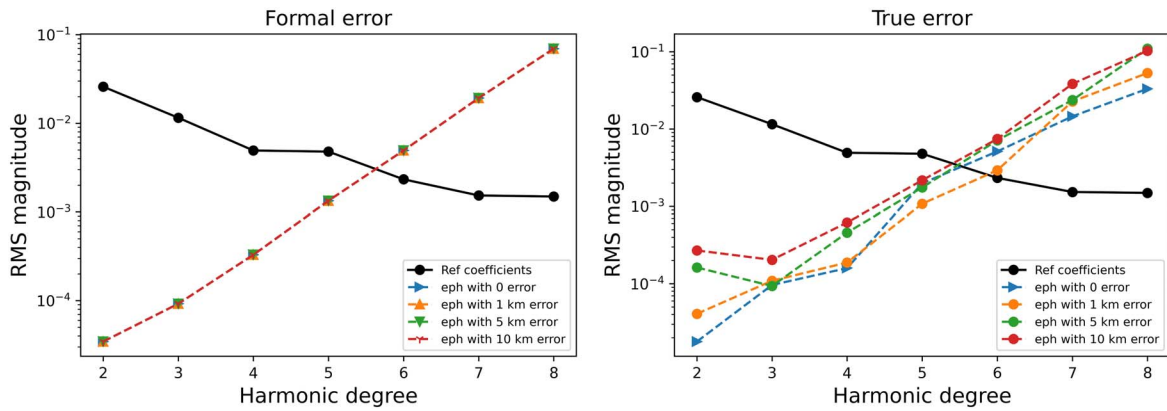


Figure 13. The degree rms magnitude spectra of the formal error and true error for different ephemeris errors for case 4 listed in Table 4.

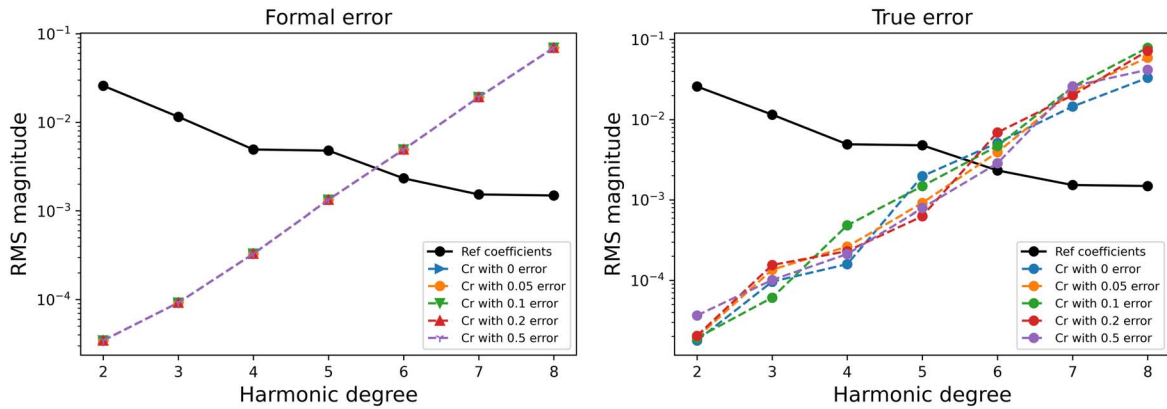


Figure 14. The degree rms magnitude spectra of the formal error and true error for case 5 in Table 4.

0.1, 0.2 and 0.5 for both probes, at the same time. The results are shown in Figure 14.

As shown in Figure 14, the effect of C_r with different errors also cannot be assessed based on the formal error alone. From the

true error, we can see that the C_r mis-modeling effect affects the accuracy of estimating the gravity field model. Mis-modeling C_r at different levels has various effects on the solutions; therefore, the accurate modeling of the solar radiation pressure is necessary.

4. Discussion and Conclusion

In this paper, we propose an inter-satellite observation measurement mode between twin orbital probes, in addition to the 2W classical Earth-probe tracking, to model the gravity field of comet 133P in the frame of the future Chinese mission to this main belt body. We considered several error sources: measurement noise levels, solar radiation pressure, and an ephemeris error for the comet orbit.

Our results indicate that these twin probes radio-links are more sensitive to the gravity field of the comet than the classical 2W-only tracking from Earth, because the inter-satellite link is only sensitive to the tidal acceleration between the probes, while in the 2W-only mode, the motion between the comet and Earth dominates the signal. Therefore, the signal-over-noise ratio is relatively higher. But conversely, the inter-satellite mode cannot be used alone, as only the differential velocity between them is sensed. Tracking data from Earth is also needed to get absolute accelerations. A twin orbit altitude of 8 km with respect to the 133P center, about 6 km to the surface, permits the modeling of the gravity field up to degree and order 5, but such a low altitude must be balanced with security concerns about the survivability of the probe in a probably dust-rich environment. The orbital altitude needs to be adjusted appropriately for future exploration mission. Gao et al. (2021a) analyzed the uncertainties of GM and C_r for three orbit altitudes of 100, 150, and 200 km altitudes, treating 133P as point-mass. Observation data from ground station combined with onboard range data can significantly reduce the uncertainties in GM and C_r . The gravity field model and rotation of 133P were estimated by using simulated two-way Earth-orbiter and orbiter-lander range rate data (Gao et al. 2021b). The orbiter-lander data will facilitate the solution of the rotation parameters, as the lander is by definition on the comet surface. However, the precision of the gravity field model estimated in this paper is slightly higher, because the inter-satellite observation data are more sensitive to the gravity recovery.

There are still some ways of improvement in this simulation experiment, but there is currently very little reliable information about 133P. First, there is unknown about its space environment. The modeling of its outgassing, and its impact on orbit of probe, need to be considered accurately. Second, the shape and rotation parameters of 133P are subject to large uncertainties. Third, the modeling of the gravity field may not be limited to inter-satellite observation mode, but may be use data from multiple sources in order to obtain more reliable information. Lastly, there are many sources of error in the actual processing, such as atmospheric correction and correction of ground station coordinates, etc. As future exploration missions are carried out and observation data are accumulated, the shape, gravity field model and orientation of 133P will be better constrained.

Acknowledgments

We sincerely appreciate the reviewers and the editor for their constructive comments, which greatly improved our submission manuscript. This work is supported by the National Natural Science Foundation of China (42241116 and U1831132). J. Yan is supported by the Macau Science and Technology Development Fund (No. SKL-LPS(MUST)-2021-2023) and the 2022 Project of Xinjiang Uygur Autonomous Region of China for Heaven Lake Talent Program; Z. Wang is supported by the Chinese Academy of Sciences Foundation of the young scholars of western (2020-XBQNXZ-019); and J.P. Barriot is supported by a DAR grant in planetology from the French Space Agency (CNES).

Appendix The Reference Gravity Field Model of 133P

In the appendix we give the reference gravity field model of 133P that is generated from the shape model. The gravity field model of 133P is given up to degree and order of 8.

Table A1

The Reference Gravity Field Model of 133P Generated from a Shape Model

n	m	\bar{C}	\bar{S}	n	m	\bar{C}	\bar{S}
0	0	1.00E+00	0.00E+00	6	2	1.03E-03	-2.10E-03
1	0	0.00E+00	0.00E+00	6	3	2.90E-03	4.07E-03
1	1	0.00E+00	0.00E+00	6	4	-6.47E-04	2.81E-04
2	0	-2.66E-02	0.00E+00	6	5	-2.39E-04	3.32E-03
2	1	3.83E-02	-1.72E-02	6	6	3.31E-04	5.01E-03
2	2	-1.98E-02	2.19E-02	7	0	1.48E-03	0.00E+00
3	0	1.13E-02	0.00E+00	7	1	1.01E-03	3.79E-04
3	1	1.12E-02	1.29E-02	7	2	-4.78E-04	-3.31E-03
3	2	-1.19E-02	-7.36E-03	7	3	1.15E-03	2.08E-03
3	3	-1.67E-02	-6.08E-03	7	4	1.08E-03	-1.74E-03
4	0	-1.09E-02	0.00E+00	7	5	-1.59E-03	-2.32E-04
4	1	9.64E-04	-2.23E-03	7	6	2.13E-03	9.31E-04
4	2	3.74E-03	2.79E-03	7	7	-1.63E-03	1.96E-04
4	3	-5.94E-03	5.78E-03	8	0	-2.23E-04	0.00E+00
4	4	-7.63E-04	-1.73E-03	8	1	-1.50E-04	-4.59E-04
5	0	-4.77E-03	0.00E+00	8	2	2.73E-03	-6.81E-04
5	1	3.03E-03	2.77E-03	8	3	3.61E-04	-2.06E-03
5	2	-3.08E-03	-6.04E-04	8	4	2.59E-04	1.82E-03
5	3	-7.81E-03	-7.95E-03	8	5	2.07E-03	1.74E-03
5	4	-6.79E-03	2.47E-03	8	6	-2.10E-03	-3.00E-04
5	5	-2.94E-03	4.11E-03	8	7	-4.28E-04	-1.76E-04
6	0	1.42E-03	0.00E+00	8	8	-3.09E-03	-2.73E-04
6	1	9.83E-04	1.38E-04				

ORCID iDsJian-Guo Yan  <https://orcid.org/0000-0003-2612-4776>**References**

Benedetti, G., Bloise, N., Boi, D., et al. 2019, *AcAau*, **154**, 238
Boehnhardt, H., Sekanina, Z., Fiedler, A., et al. 1998, *HiA*, **11**, 233
Chang, S. Q., Huang, Y., Li, P. J., Hu, X. G., & Fan, M. 2016, *RAA*, **16**, 010
Cheng, A. F., Santo, A., Heeres, K., et al. 1997, *JGRE*, **102**, 23695
Chesley, S. R., French, A. S., Davis, A. B., et al. 2020, *JGRE*, **125**, e2019JE006363
Elst, E. W., Pizarro, O., Pollas, C., et al. 1996, *IAUC*, **6456**, 1
Eshagh, M., & Šprlák, M. 2016, *CeMDA*, **124**, 127
Gao, W. T., Yan, J. G., Jin, W. T., et al. 2021a, *RAA*, **21**, 016
Gao, W. T., Yan, J. G., Wang, B., et al. 2021b, *MNRAS*, **505**, 103

Gao, W. T., Yan, J. G., Wang, B., et al. 2023, *SSPMA*, **53**, 259513
Genova, A., & Petricca, F. 2021, *JGCD*, **44**, 1068
Glassmeier, K. H., Boehnhardt, H., Koschny, D., Kührt, E., & Richter, I. 2007, *SSRv*, **128**, 1
Godard, B., Budnik, F., Bellei, G., Muñoz, P., & Morley, T. 2017, in Proc. 26th Int. Symp. on Space Flight Dynamics—26th ISSFD (Matsuyama: ISSFD)
Hsieh, H. H., Jewitt, D., & Fernández, Y. R. 2009, *ApJL*, **694**, L111
Hsieh, H. H., Jewitt, D., Lacerda, P., Lowry, S. C., & Snodgrass, C. 2010, *MNRAS*, **403**, 363
Hsieh, H. H., Jewitt, D. C., & Fernández, Y. R. 2004, *AJ*, **127**, 2997
Jewitt, D., Agarwal, J., Weaver, H., Mutchler, M., & Larson, S. 2013, *ApJL*, **778**, L21
Jewitt, D., Ishiguro, M., Weaver, H., et al. 2014, *AJ*, **147**, 117
Kaula, W. M. 1966, *Theory of Satellite Geodesy* (Waltham: Blaisdell Publishing Company)
Konopliv, A., Asmar, S., Park, R., et al. 2014, *Icar*, **240**, 103
Konopliv, A., Park, R., Vaughan, A., et al. 2018, *Icar*, **299**, 411
Lauretta, D. S., Bartels, A. E., Barucci, M. A., et al. 2015, *M&PS*, **50**, 834
Lauretta, D. S., Hergenrother, C. W., Chesley, S. R., et al. 2019, *Sci*, **366**, eaay3544
Leonard, J., Jones, B., Villalba, E., & Born, G. 2012, in *AIAA/AAS Astrodynamics Specialist Conf.* (Minneapolis, MI: AIAA), 4877
Liu, P., Hou, X. Y., Tang, J. S., & Liu, L. 2014, *RAA*, **14**, 1307
McMahon, J., Scheeres, D., Hesar, S., et al. 2018, *SSRv*, **214**, 43
Miller, J. K., Konopliv, A., Antreasian, P., et al. 2002, *Icar*, **155**, 3
Montenbruck, O., & Gill, E. 2001, *Obs*, **121**, 182
Park, R. S., Konopliv, A. S., Yuan, D. N., et al. 2015, in *A high-resolution spherical harmonic degree 1500 lunar gravity field from the GRAIL mission in American Geophysical Union Fall Meeting* (San Francisco, CA: AGUFM), G41B
Pätzold, M., Andert, T., Hahn, M., et al. 2016, *Natur*, **530**, 63
Psiaki, M. L. 2011, *JGCD*, **34**, 1285
Russell, C. T., & Raymond, C. A. 2011, *The Dawn Mission to Minor Planets 4 Vesta and 1 Ceres* (Berlin: Springer), 3
Scheeres, D., Gaskell, R., Abe, S., et al. 2006, in *AIAA/AAS Astrodynamics Specialist Conf. and Exhibit* (Keystone, CO: AIAA), 6661
Sharkey, B. N. L., Reddy, V., Malhotra, R., et al. 2021, *ComEE*, **2**, 231
Turan, E., Speretta, S., & Gill, E. 2022a, *AcAau*, **193**, 56
Turan, E., Speretta, S., & Gill, E. 2022b, in *Radiometric Autonomous Navigation for Cislunar Satellite Formations in 10th Workshop on Satellite Navigation Technology, NAVITEC 2022* (The Netherlands: ESA)
Watanabe, S., Hirabayashi, M., Hirata, N., et al. 2019, *Sci*, **364**, 268
Watanabe, S., Tsuda, Y., Yoshikawa, M., et al. 2017, *SSRv*, **208**, 3
Yamamoto, K., Otsubo, T., Matsumoto, K., et al. 2020, *EP&S*, **72**, 85
Ye, M., Li, F., Yan, J. G., et al. 2021, *RemS*, **13**, 3747
Yim, J. R., Crassidis, J. L., & Junkins, J. L. 2004, in Proc. AAS Space Flight Mechanics Meeting (Maui: AAS)
Yoshikawa, M., Kawaguchi, J., Fujiwara, A., & Tsuchiyama, A. 2015, *Asteroids IV*, Vol. 1 (Tucson, AZ: Univ. Arizona Press), 1
Yu, L. L., Hsia, C. H., & Ip, W.-H. 2020, *AJ*, **159**, 66
Zuber, M. T., Smith, D. E., Watkins, M. M., et al. 2013, *Sci*, **339**, 668